Electronic Supplementary Material (ESI) for Nanoscale.
This journal is © The Royal Society of Chemistry 2024

A convenient protonated strategy for constructing nanodrugs from hydrophobic drug-inhibitor conjugates to reverse tumor multidrug resistance

Penghui Wang,[a] Yulin Wang,[a] Xuelin Xia,[a] Jingchun Wu,[b] Jintang Lin,[b] Wei Huang*[a] and Deyue Yan*[a]

[a]*School of Chemistry and Chemical Engineering, State Key Laboratory of Metal Matrix Composites, Shanghai Jiao Tong University, Shanghai 200240, China*

[b]*Zhejiang Haobang Chemical Co., LTD, 26 Luyin Road, Quzhou Hi-Tech Industrial Park, Zhejiang 324100, China*

E-mail: hw66@sjtu.edu.cn; dyyan@sjtu.edu.cn

Characterization: ^{1}H, ^{13}C, and ^{19}F NMR spectra were measured by the Bruker AVANCE III HD 400 or 500 MHz spectrometer. LC-MS spectra were performed with Acquity 2D-UPLC/Acquity UPC2-Xevo G2-XS QTOF (Waters, USA). Pharmacokinetic samples were analyzed by Acquity UPLC H-class/Xevo TQ-XS (Waters, USA). The UV-Vis absorption spectrum was measured with a Thermo Electron-EV300 UV-Vis spectrophotometer. The size distribution of the assembly was measured using a dynamic light scattering (DLS) apparatus (Malvern Zetasizer Nano S, UK). The zeta potential was investigated by a Brookhaven NanoBrook-Omni High Sensitivity Zeta Potentiometer and Particle Size Analyzer. Transmission electron microscopy (TEM) was performed using a Tecnai G2 Spirit Biotwin instrument (Thermo Fisher, USA) at 120 kV. Scanning transmission electron microscopy energy dispersive spectroscopy (STEM-EDS) was carried out by Talos F200X G2 transmission electron microscopy (Thermo Fisher, USA). CMC was measured by Steady-State & Time-Resolved Fluorescence Spectrofluorometer (PTI, USA). Laser confocal imaging was investigated on a Leica TCS SP8 STED 3X Super-resolution multiphoton confocal microscope (Leica, Germany). The flow cytometry analysis was performed on a BD LSR Fortessa flow cytometer (BD, USA).

1 Syntheses of Zos-ss-COOH, PTX-ss-Zos and PTX-ss-Zos·HCl

1.1 Syntheses of Zos-ss-COOH

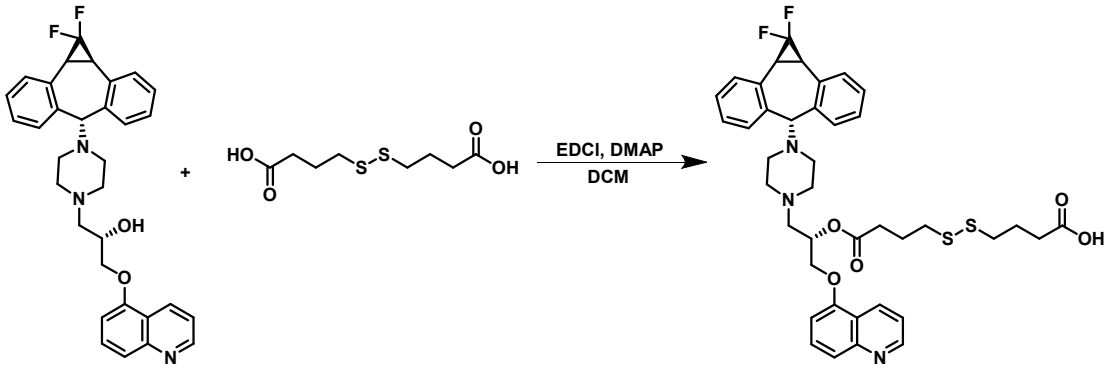

Zos Zos-ss-COOH

4,4'-dithiodibutyric acid (476 mg, 2 mmol), EDCl (575.1 mg, 3 mmol), and DMAP (24.4 mg, 0.2 mmol) were added in anhydrous CH_2Cl_2 (10 mL) and the mixture was stirred at 25℃ for 0.5 h under N_2 atmosphere. Then Zos (527 mg, 1 mmol) was added and the resulting solution was stirred for 72 h. Thereafter, the reaction mixture was washed with saturated NaCl solution, the organic phase was collected and purified by column chromatography (CH_2Cl_2:CH_3OH, 30:1, v/v) to obtain Zos-ss-COOH as a white powder (616.28 mg, yield 82.5%).

^{1}H NMR (500 MHz, DMSO) δ 8.89 (d, *J* = 1.7 Hz, 1H), 8.44 (d, *J* = 8.2 Hz, 1H), 7.69 – 7.59 (m, 2H), 7.50 (dd, *J* = 7.9, 3.8 Hz, 1H), 7.27 – 7.13 (m, 9H), 7.06 (d, *J* = 7.5 Hz, 1H), 5.47 (s, 1H), 4.42 – 4.20 (m, 2H), 4.00 (s, 1H), 3.60 (s, 1H), 3.34 (d, *J* = 12.2 Hz, 2H), 2.75 – 2.62 (m, 8H), 2.46 – 2.39 (m, 3H), 2.36 – 2.26 (m, 5H), 1.91 – 1.80 (m, 5H).

^{19}F NMR (376 MHz, $CDCl_3$) δ -123.49 (d, *J* = 144.6 Hz), -139.03 (d, *J* = 144.6 Hz).

^{13}C NMR (126 MHz, DMSO) δ 174.36, 174.32, 173.24, 172.36, 154.02, 151.24, 148.97, 142.74, 132.85, 130.35, 130.04, 129.97, 128.83, 128.29, 127.98, 121.80, 121.20, 120.44, 106.28, 76.93, 69.56, 69.03, 57.94, 55.37, 54.06, 53.83, 52.26, 51.80, 37.38, 37.36, 37.34, 37.18, 37.05, 32.75, 32.58, 32.56, 32.23, 28.95, 28.88, 28.82, 24.65, 24.47, 24.41, 24.39.

HRMS: $[M+H]^+$ m/z calculated for 748.2685, found 748.2683.

1.2 Synthesis of PTX-ss-Zos Conjugate.

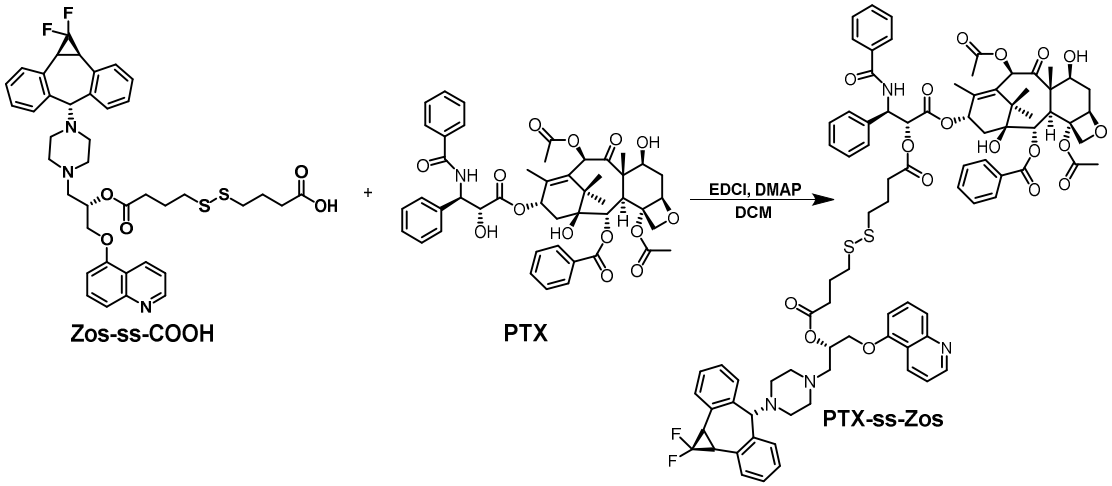

A mixture of Zos-ss-COOH (747mg, 1 mmol), EDC·HCl (287.55 mg, 1.5 mmol), and DMAP (24.4 mg, 0.2 mmol) were well stirred together at 25℃ in anhydrous CH_2Cl_2 (10 mL) for 30 min under N_2 atmosphere. Then PTX (854 mg, 1 mmol) was added and the resulting solution was stirred at 25℃ overnight. After completion of the reaction, the reaction mixture was washed with saturated NaCl solution, the organic phase was collected and purified by column chromatography (CH_2Cl_2:CH_3OH, 60:1, v/v) to obtain Zos-ss-COOH as a white powder (1126.38 mg, yield 71.2%).

^{1}H NMR (500 MHz, $CDCl_3$) δ 8.85 (d, *J* = 2.7 Hz, 1H), 8.52 (d, *J* = 8.2 Hz, 1H), 8.16 (d, *J* = 7.4 Hz, 2H), 7.76 (d, *J* = 7.4 Hz, 2H), 7.69 (d, *J* = 8.5 Hz, 1H), 7.63 – 7.56 (m, 2H), 7.52 (t, *J* = 7.6 Hz, 2H), 7.49 – 7.31 (m, 10H), 7.29 – 7.24 (m, 3H), 7.17 (ddd, *J* = 21.2, 15.1, 7.9 Hz, 6H), 6.87 (d, *J* = 7.7 Hz, 1H), 6.34 (s, 1H), 6.28 (t, *J* = 8.7 Hz, 1H), 6.02 (dd, *J* = 9.1, 2.6 Hz, 1H), 5.72 (d, *J* = 7.0 Hz, 1H), 5.54 (d, *J* = 2.9 Hz, 2H), 4.99 (d, *J* = 9.1 Hz, 1H), 4.47 (dd, *J* = 10.4, 6.9 Hz, 1H), 4.35 (dd, *J* = 13.5, 5.7 Hz, 2H), 4.29 – 4.19 (m, 2H), 3.93 (s, 1H), 3.85 (d, *J* = 6.9 Hz, 1H), 3.20 (d, *J* = 12.2 Hz, 2H), 2.72 (d, *J* = 6.1 Hz, 2H), 2.66 (t, *J* = 7.1 Hz, 3H), 2.60 – 2.52 (m, 5H), 2.49 – 2.38 (m, 10H), 2.32 (s, 2H), 2.22 (s, 4H), 2.06 – 1.86 (m, 10H), 1.71 (s, 3H), 1.25 (s, 3H), 1.16 (s, 3H).

^{19}F NMR (471 MHz, $CDCl_3$) δ -123.48 (d, *J* = 144.4 Hz), -138.95 (d, *J* = 144.4 Hz).

^{13}C NMR (126 MHz, $CDCl_3$) δ 203.83, 172.46, 172.02, 171.20, 169.87, 168.16, 167.42, 166.93, 153.94, 150.68, 148.86, 142.54, 142.17, 136.96, 133.65, 132.93, 132.73, 132.02, 130.87, 130.24, 129.64, 129.39, 129.31, 129.14, 128.75, 128.71, 128.56, 128.53, 127.99, 127.60, 127.20, 126.58, 121.87, 120.82, 120.44, 105.26, 84.47, 81.12, 78.97, 77.91, 76.47, 75.63, 75.13, 74.03, 72.06, 71.93, 69.59, 68.60, 60.45, 58.49, 58.20, 54.18, 53.50, 52.74, 52.19, 45.67, 43.24, 37.47, 37.02, 35.65, 32.83, 31.89, 29.72, 29.04, 28.97, 28.89, 26.81, 24.30, 23.82, 22.73, 22.17, 21.08, 20.86, 14.83, 14.22, 9.68, 1.05.

HRMS: $[M+H]^+$m/z calculated for 1583.5889, found 1583.5986.

1.3 Synthesis of PTX-ss-Zos•HCl.

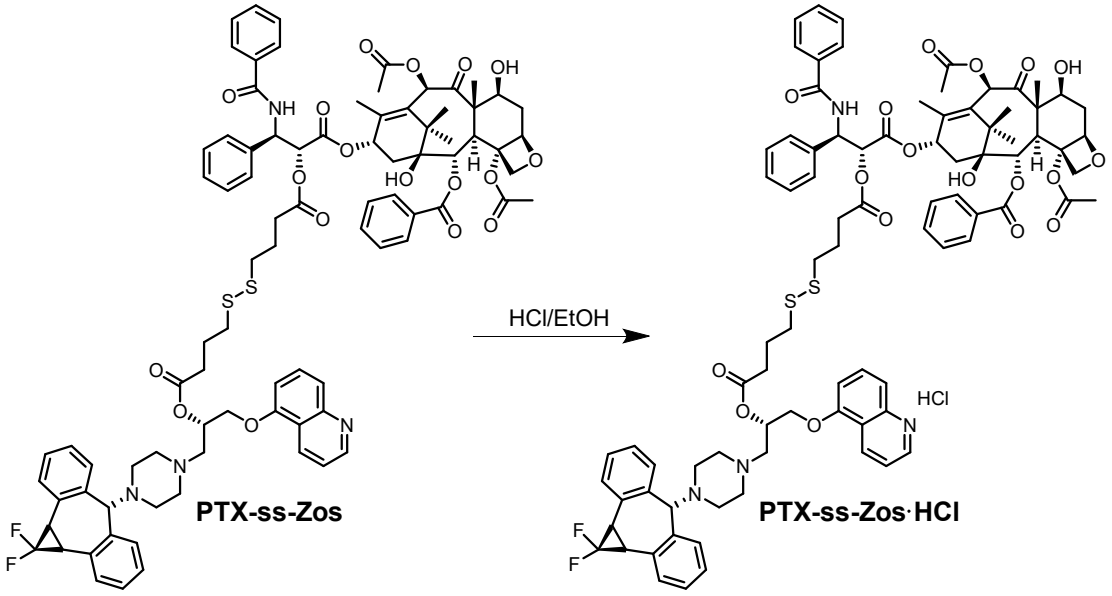

To a stirred solution of PTX-ss-Zos (100 mg, 0.063 mmol) in 5 mL dry ethyl acetate was added 24 μL HCl/EtOH (8 mol/L) at 25℃. The resulting solution continued to stir for 1 hour and then filtered. The filter cake was washed with cold ethyl acetate, and dried under vacuum at room temperature to afford the PTX-ss-Zos·HCl as a light-yellow solid (82 mg, yield 80.3%).

^{1}H NMR (500 MHz, DMSO) δ 11.74 (s, 1H), 9.43 (d, *J* = 8.3 Hz, 1H), 9.30 (d, *J* = 5.0 Hz, 2H), 8.09 – 7.96 (m, 6H), 7.90 (t, *J* = 8.5 Hz, 2H), 7.75 (t, *J* = 7.3 Hz, 1H), 7.67 (t, *J* = 7.5 Hz, 2H), 7.57 – 7.40 (m, 10H), 7.32 – 7.15 (m, 8H), 6.29 (s, 1H), 5.81 (t, *J* = 7.6 Hz, 2H), 5.51 (t, *J* = 8.8 Hz, 1H), 5.46 – 5.39 (m, 2H), 4.91 (d, *J* = 10.0 Hz, 1H), 4.59 – 4.47 (m, 4H), 4.01 (dd, *J* = 14.9, 8.8 Hz, 3H), 3.73 (s, 3H), 3.61 – 3.40 (m, 7H), 3.24 – 3.14 (m, 1H), 2.64 – 2.54 (m, 6H), 2.46 (dd, *J* = 15.5, 8.0 Hz, 3H), 2.23 (d, *J* = 5.1 Hz, 3H), 2.18 – 2.07 (m, 4H), 1.87 – 1.73 (m, 9H), 1.67 – 1.62 (m, 1H), 1.50 (s, 3H), 1.01 (d, *J* = 14.3 Hz, 6H).

^{19}F NMR (471 MHz, DMSO) δ -122.42 (d, *J* = 143.4 Hz), -137.04 (d, *J* = 142.4 Hz).

^{13}C NMR (126 MHz, DMSO) δ 202.82, 172.63, 172.40, 172.30, 170.80, 170.47, 170.16, 169.92, 169.42, 169.22, 166.85, 166.75, 166.34, 165.68, 154.19, 145.93, 140.85, 139.83, 139.35, 137.83, 135.73, 134.57, 133.98, 133.86, 133.09, 131.94,

130.39, 130.03, 129.16, 128.75, 128.70, 128.18, 128.08, 127.96, 123.60, 121.73, 121.42, 113.73, 109.26, 84.07, 80.68, 77.17, 76.65, 75.75, 75.19, 75.07, 74.94, 73.58, 71.31, 70.88, 69.00, 67.48, 67.18, 66.82, 60.23, 60.09, 57.86, 56.49, 54.66, 49.05, 46.75, 46.52, 43.59, 43.41, 36.93, 36.53, 34.81, 32.67, 32.05, 28.94, 27.44, 26.82, 25.59, 24.27, 24.18, 24.05, 23.11, 22.29, 21.85, 21.24, 21.21, 21.14, 20.69, 19.03, 15.24, 14.56, 14.36, 11.46, 10.26, 0.57.

HRMS: $[M+H]^+$m/z calculated for 1584.5962, found 1584.5968.

2 Supplementary Figures

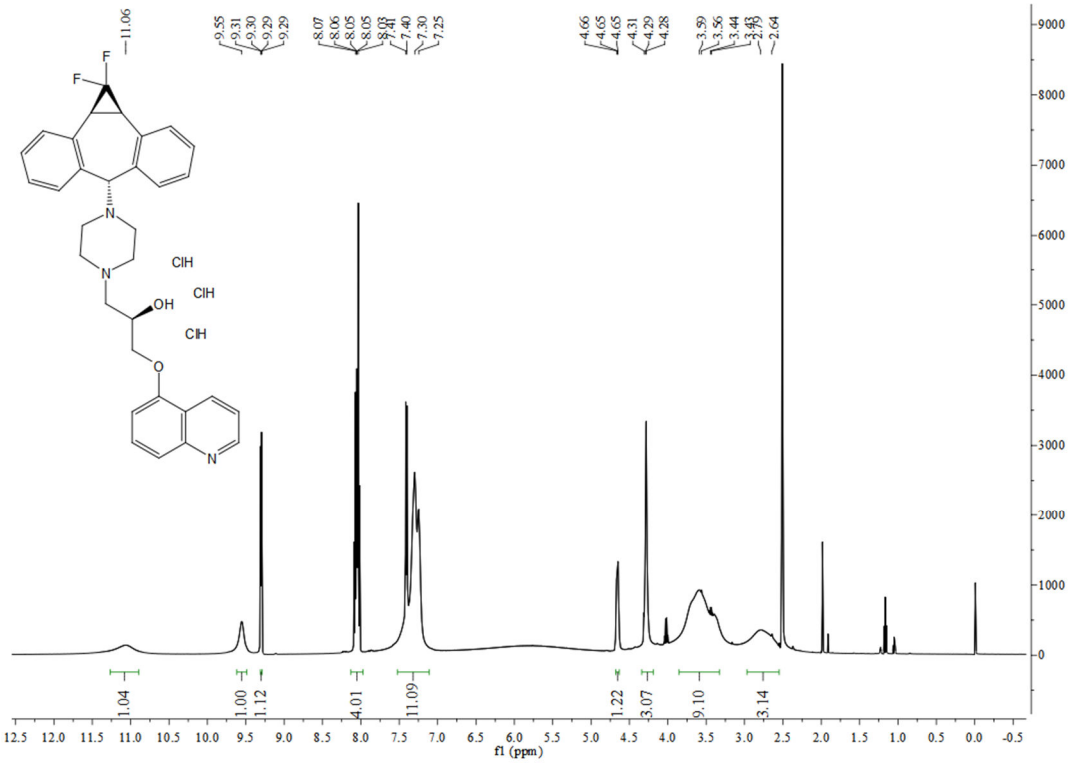

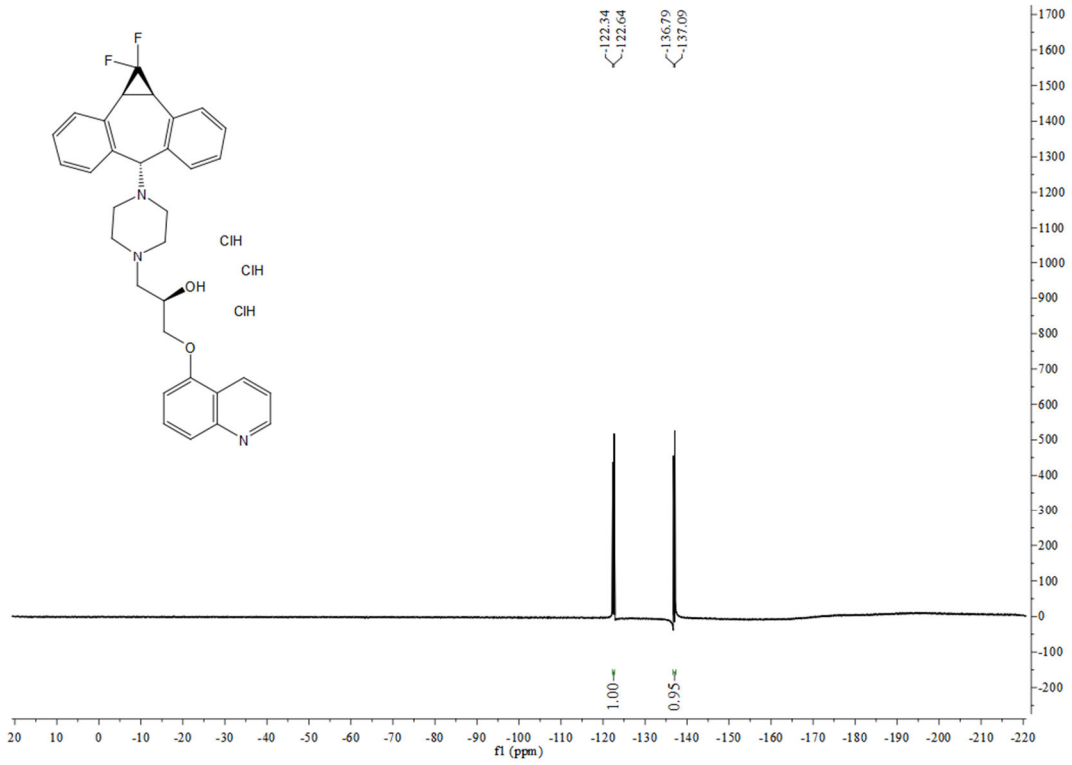

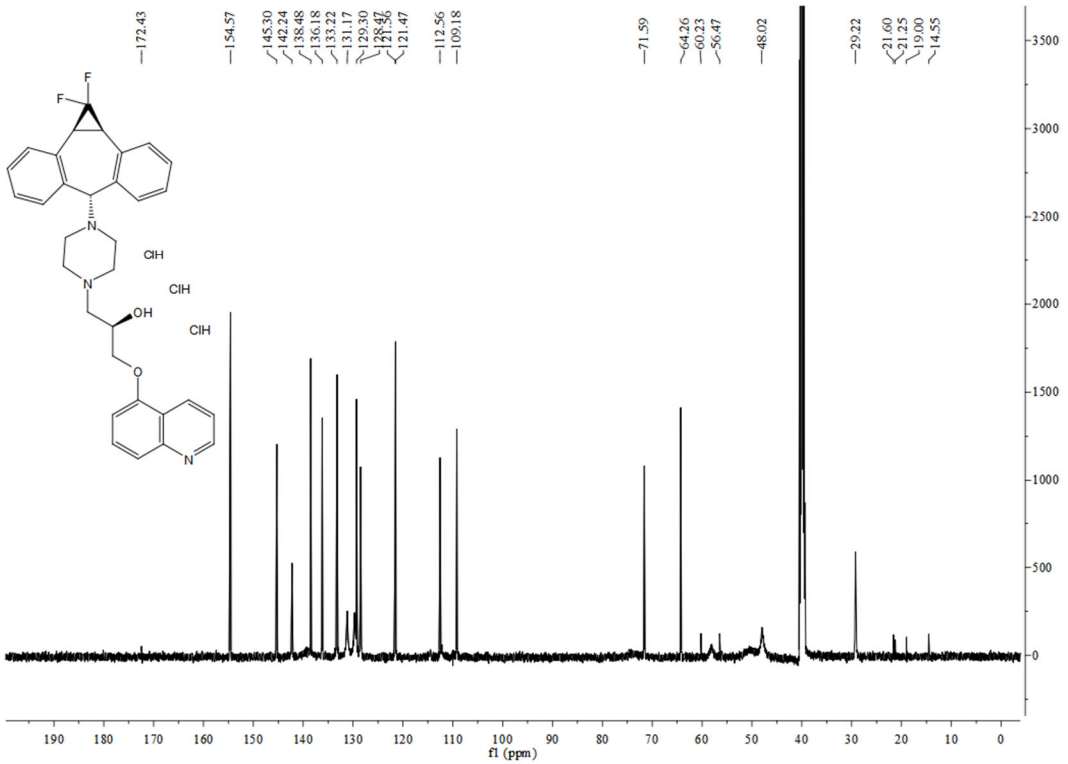

Figure S1. The ^{1}H, ^{19}F, and ^{13}C NMR spectra of Zos·3HCl in DMSO-d_6. ^{1}H NMR (500 MHz, DMSO) δ 11.06 (s, 1H), 9.55 (s, 1H), 9.30 (dd, J = 5.3, 1.2 Hz, 1H), 8.05 (dq, J = 12.9, 8.2 Hz, 4H), 7.34 (dd, J = 67.4, 16.7 Hz, 11H), 4.68 – 4.63 (m, 1H), 4.34 – 4.19 (m, 3H), 3.85 – 3.33 (m, 9H), 2.72 (d, J = 73.2 Hz, 3H). ^{19}F NMR (471 MHz, DMSO) δ -122.49 (d, J = 142.7 Hz), -136.94 (d, J = 142.4 Hz). ^{13}C NMR (126 MHz, DMSO) δ 172.43, 154.57, 145.30, 142.24, 138.48, 136.18, 133.22, 131.17, 129.69, 129.30, 128.47, 121.56, 121.47, 112.56, 109.18, 71.59, 64.26, 60.23, 56.47, 48.02, 29.22, 21.60, 21.25, 19.00, 14.55.

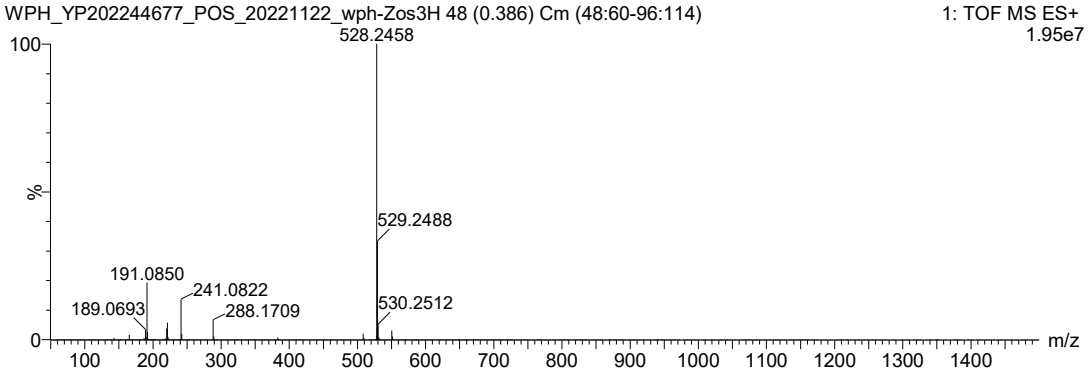

Figure S2. HRMS spectrum of Zos·3HCl ([M+H]$^{+}$m/z calculated for 528.2457, found528.2458).

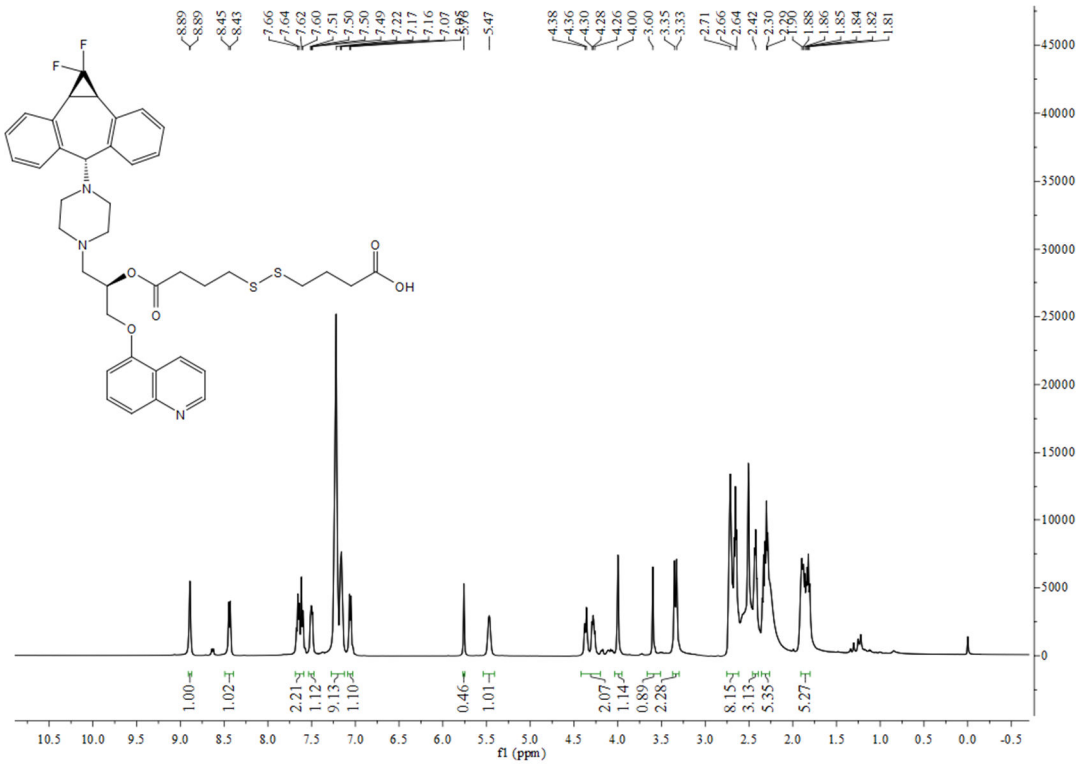
8.89
8.89
8.45
8.43
7.66
7.64
7.62
7.60
7.51
7.50
7.50
7.50
7.49
7.22
7.17
7.16
7.07
5.98
5.95
5.47
4.38
4.36
4.30
4.28
4.26
4.00
3.60
3.35
3.33
2.71
2.66
2.64
2.42
2.30
2.29
1.90
1.88
1.86
1.85
1.84
1.82
1.81
F
F
N
N
O
O
S
S
O
OH
O
N
1.00
1.02
2.21
1.12
9.13
1.10
0.46
1.01
2.07
1.14
0.89
2.28
8.15
3.13
5.35
5.27
f1 (ppm)


wph-pgp-s-H, F
-123.30
-123.68
-138.84
-139.22
F
F
N
N
O
O
S
S
O
OH
O
N
1.00
0.97
f1 (ppm)

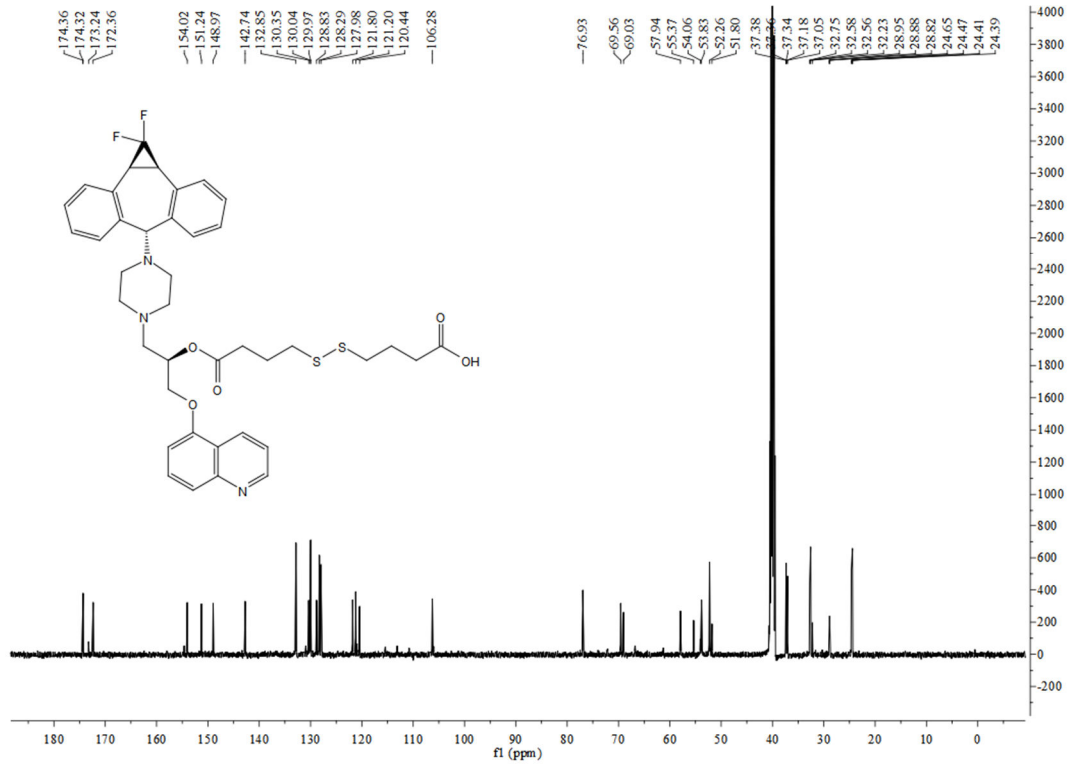

Figure S3. The ^{1}H, ^{19}F, and ^{13}C NMR spectra of Zos-ss-COOH.

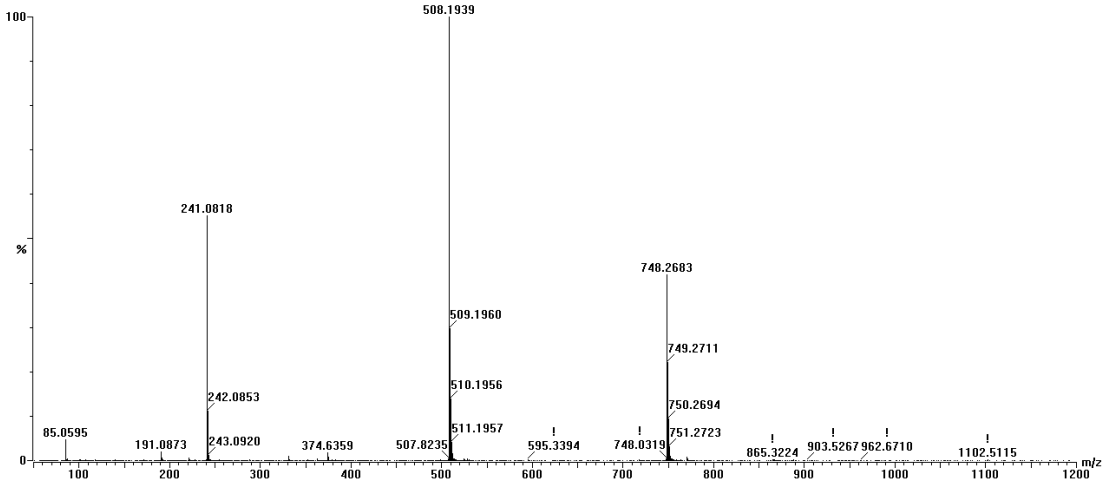

Figure S4. HRMS spectrum of Zos-ss-COOH ($[M+H]^{+}$m/z calculated for 748.2685, found 748.2683).

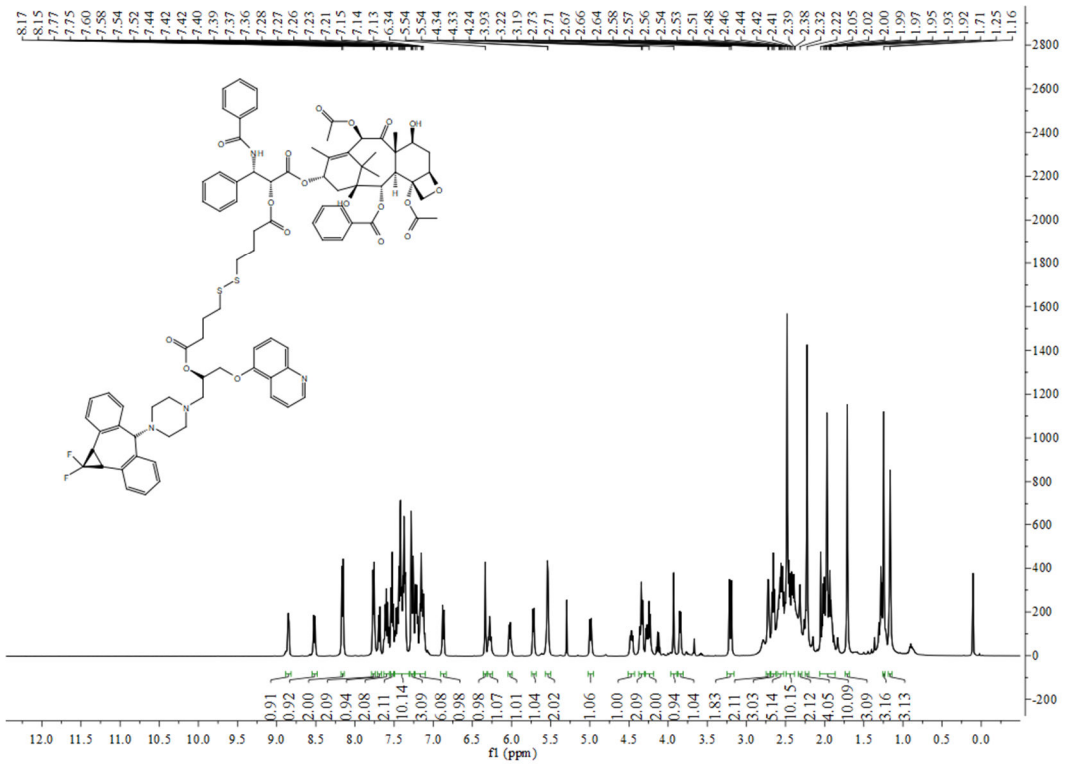
f1 (ppm)

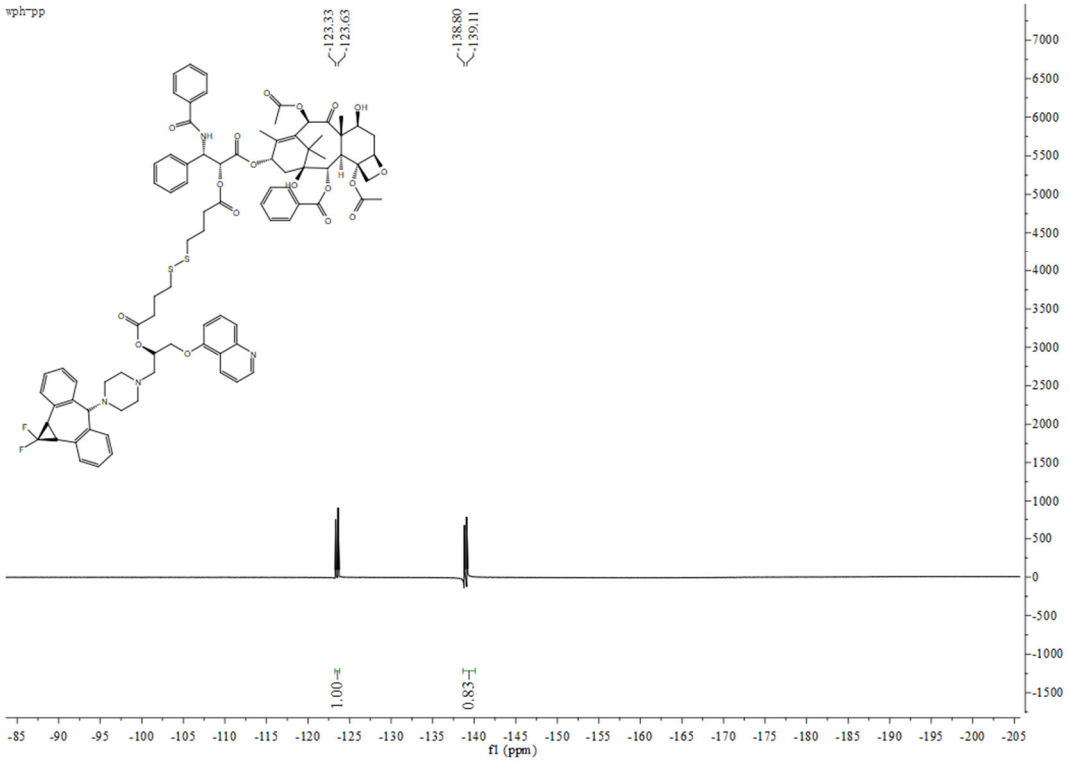
wph-pp
f1 (ppm)

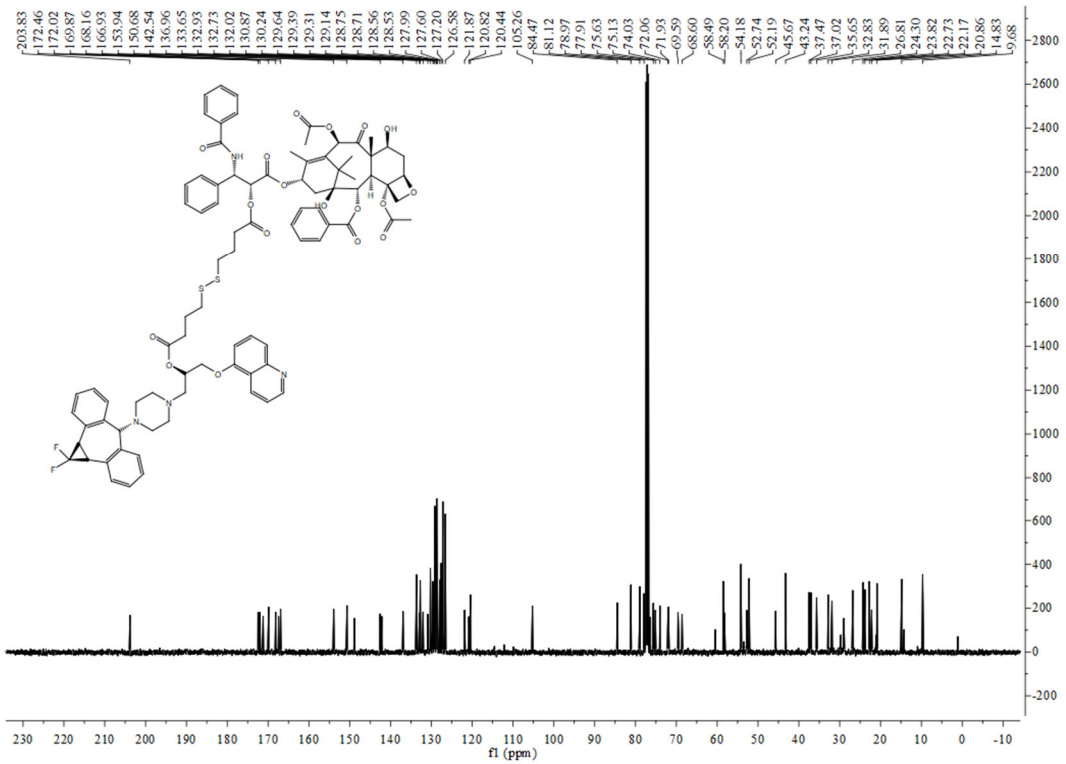

Figure S5. The ^{1}H, ^{19}F, and ^{13}C NMR spectra of PTX-ss-Zos in $CDCl_3$.

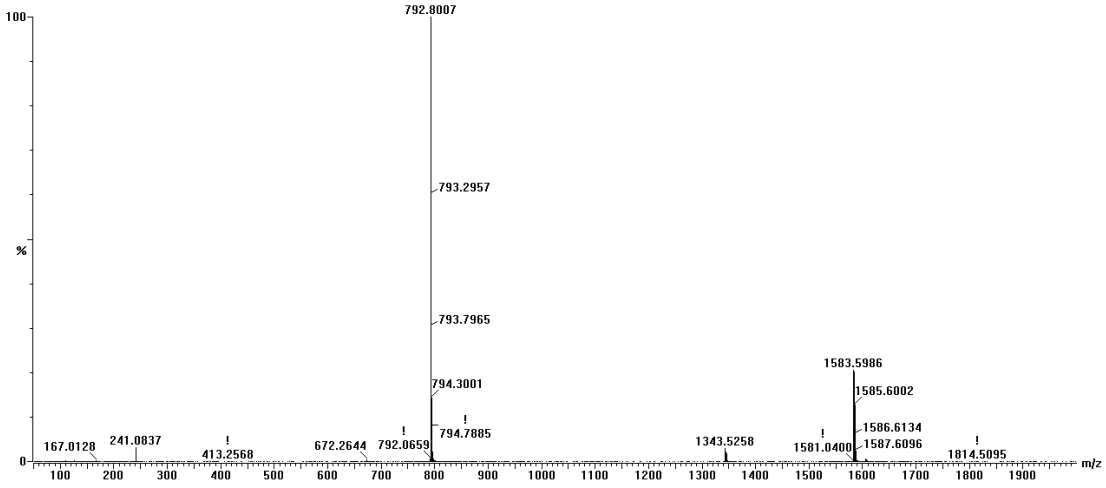

Figure S6. HRMS spectrum of PTX-ss-Zos ($[M+H]^+$m/z calculated for 1583.5889, found 1583.5986).

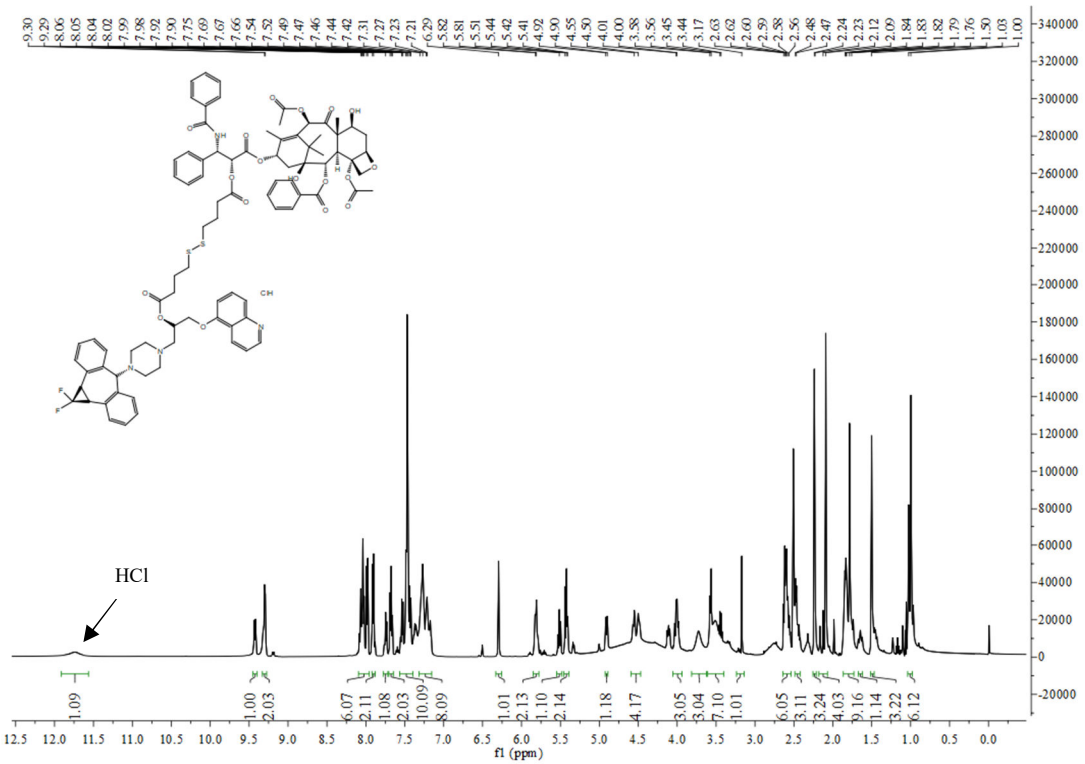
HCl
f1 (ppm)

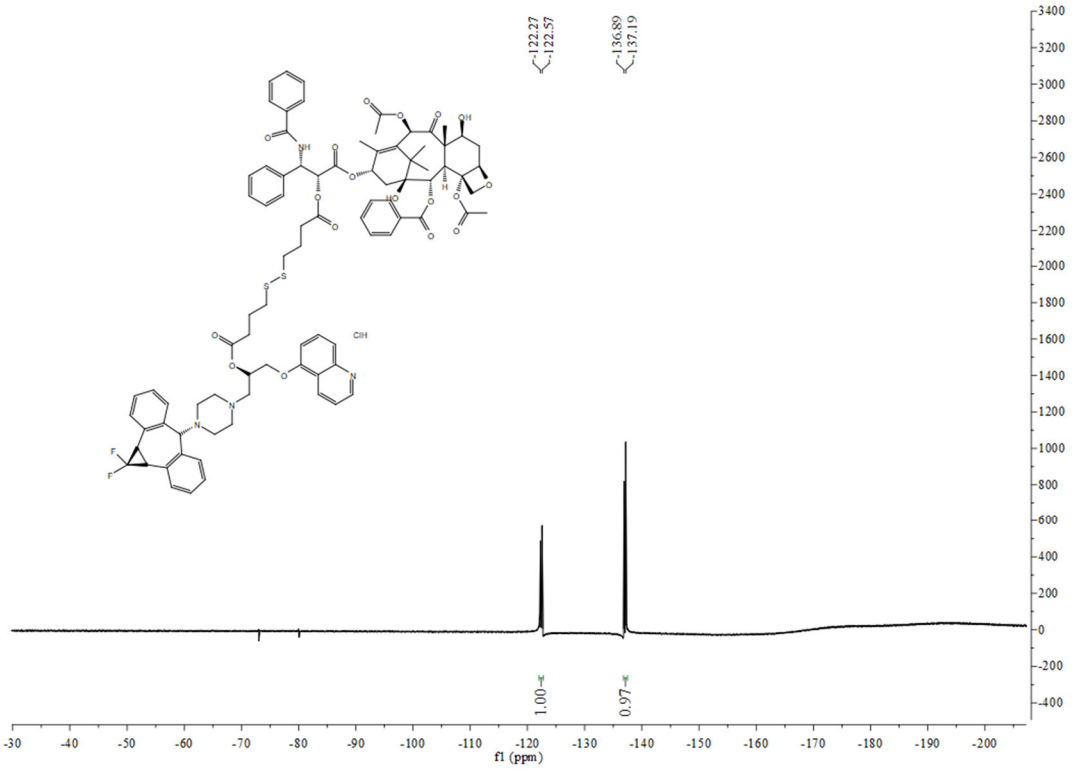
122.27
122.57
136.89
137.19
1.00
0.97
f1 (ppm)

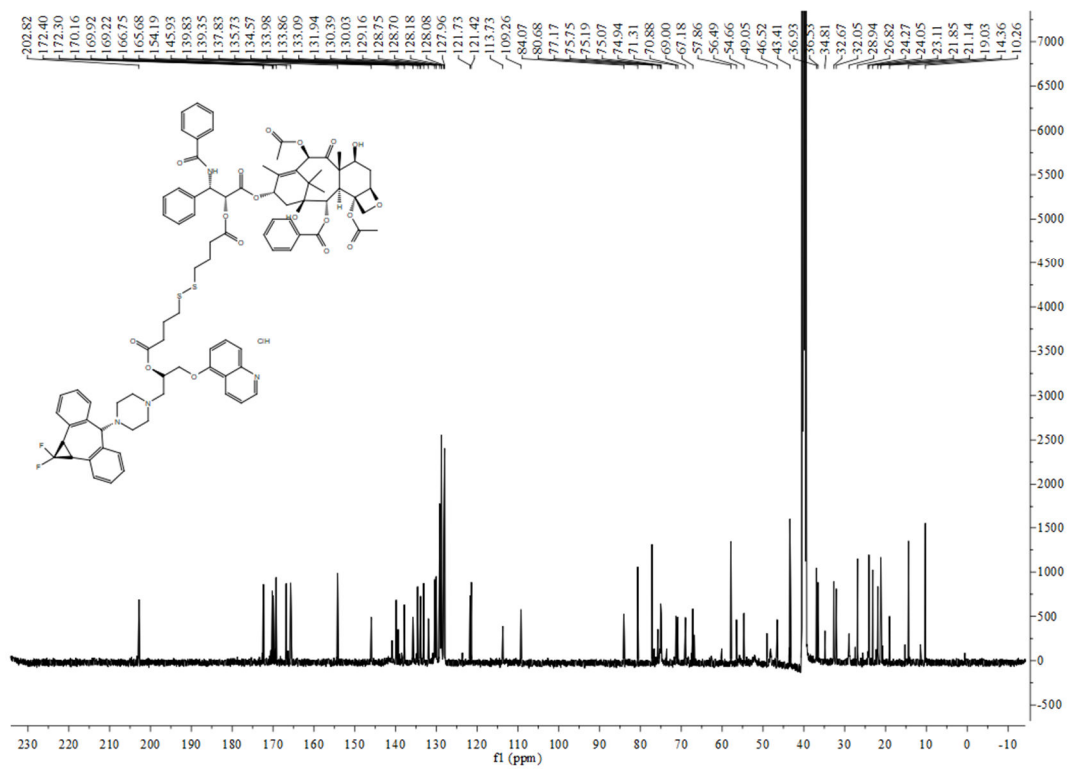

Figure S7. The ^{1}H, ^{19}F, and ^{13}C NMR spectra of PTX-ss-Zos • HCl in DMSO-d_6.

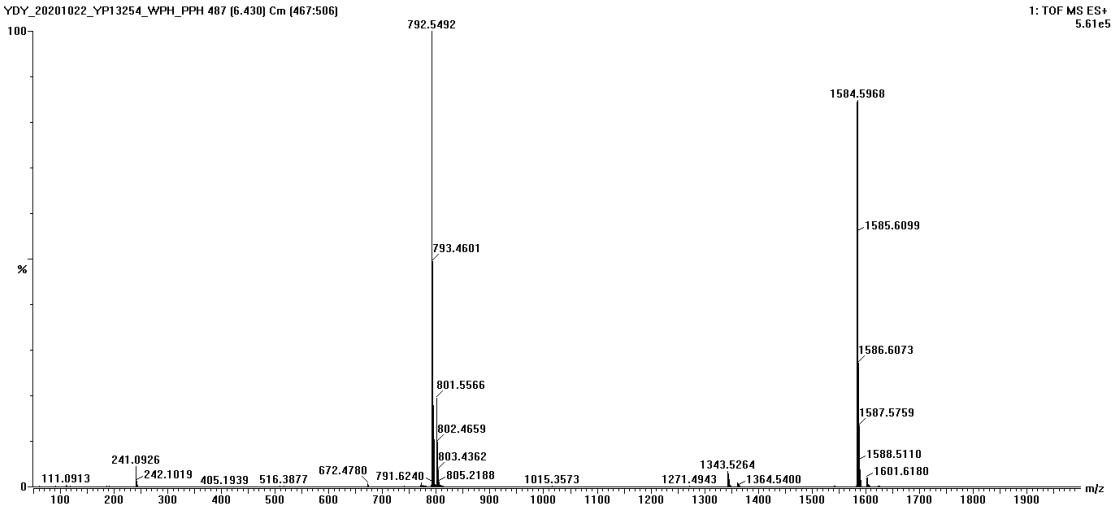

Figure S8. HRMS spectrum of PTX-ss-Zos·HCl ([M+H]$^{+}$m/z calculated for 1584.5962, found 1584.5968).

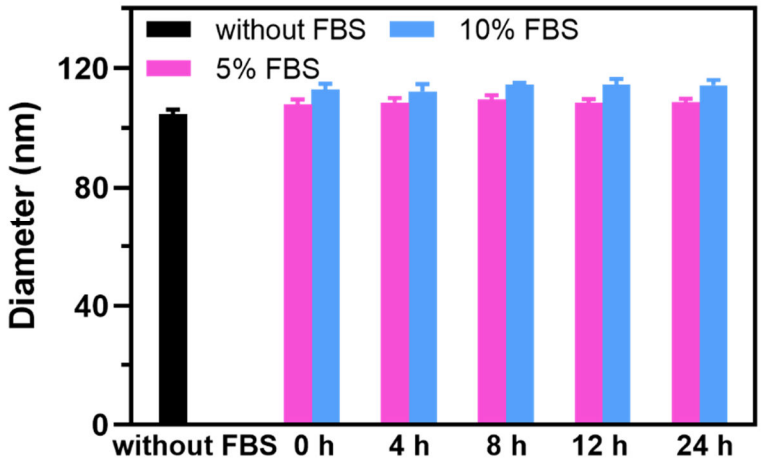

Figure S9. Time-dependent stability of PTX-ss-Zos@HCl NPs in water containing 5% or 10% FBS, respectively, was monitored by using DLS measurement.

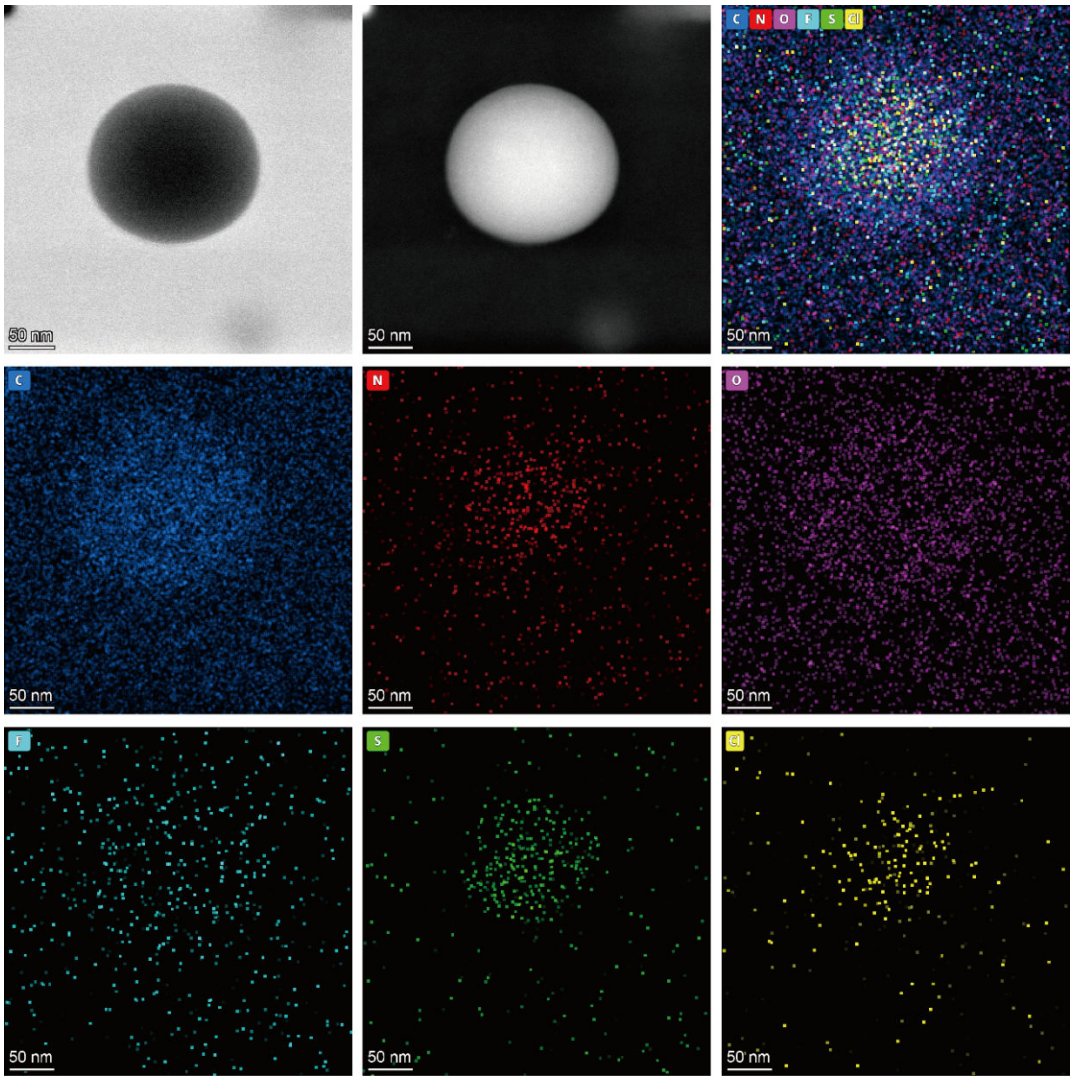

Figure S10. STEM and mapping images of PTX-ss-Zos@HCl NPs. Scale bars: 50 nm.

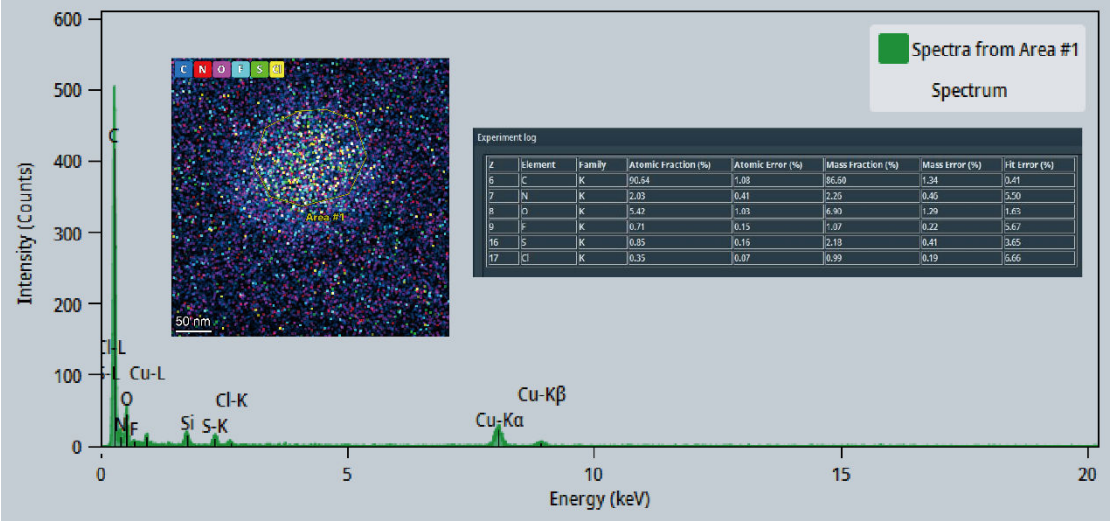

Figure S11. The energy dispersive spectroscopy (EDS) and distribution of related elements (C, N, O, F, S, Cl) in PTX-ss-Zos@HCl NPs.

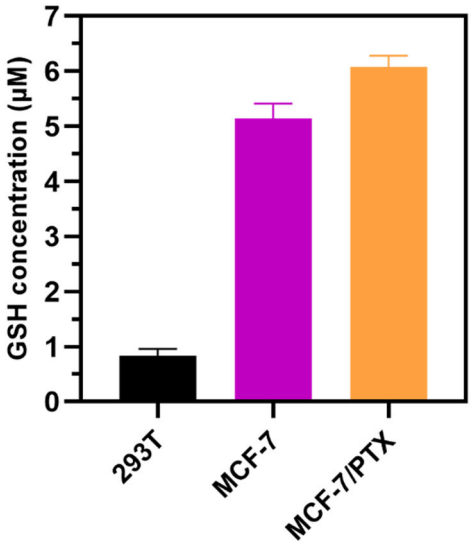

Figure S12. The level of GSH in 293T, MCF-7 and MCF-7/PTX cells (n = 3).

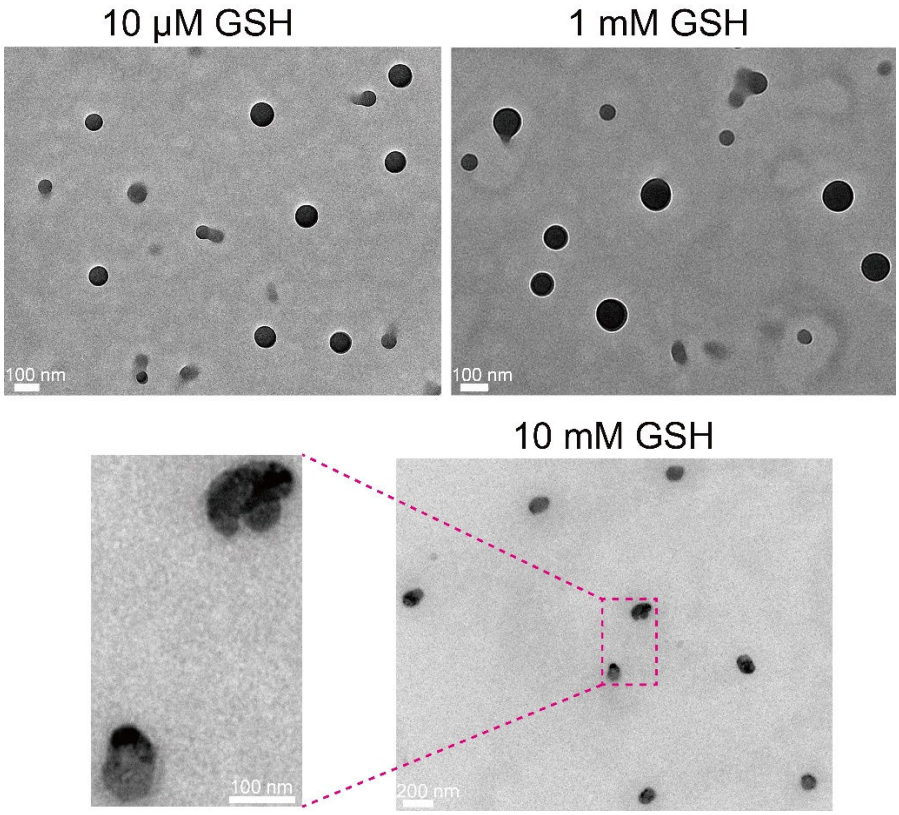

Figure S13. TEM images of PTX-ss-Zos@HCl NPs after treatment with 10 μM, 1mM, 10 mM GSH for 12h.

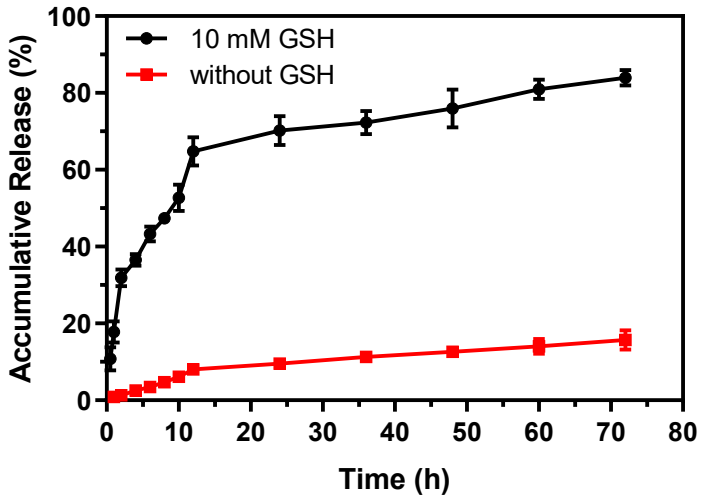

Figure S14. *In vitro* drug release of PTX-ss-Zos @HCl NPs.

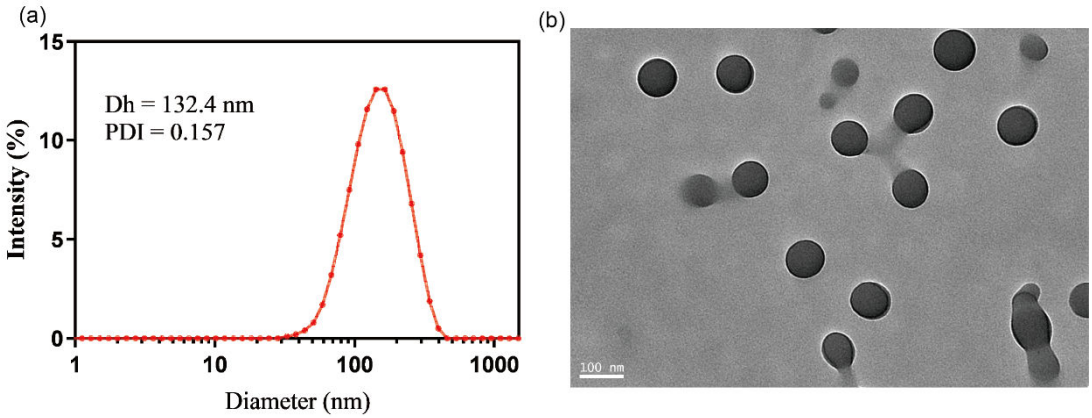

Figure S15. (a) DLS measurement and (b) TEM image of Cy5.5-loaded PTX-ss-Zos@HCl NPs. Scale bars: 100 nm.

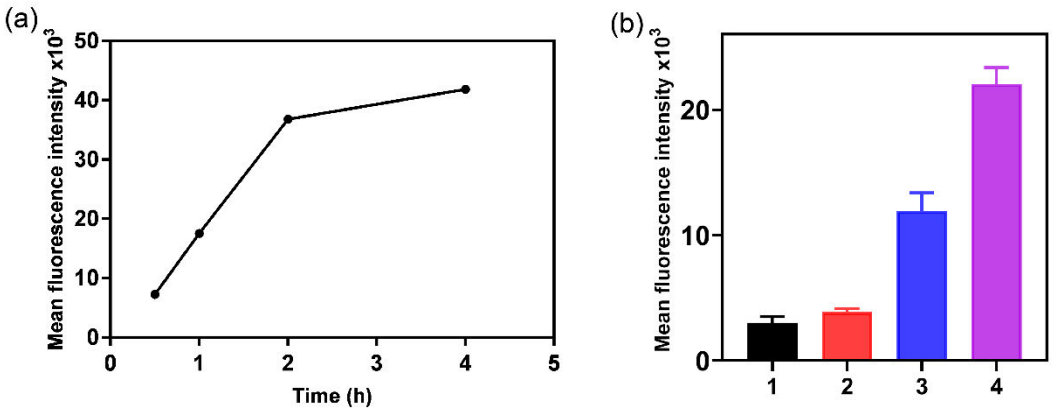

Figure S16. (a) Time-dependent fluorescence intensity profiles of Cy5.5-loaded PTX-ss-Zos @HCl NPs in MCF-7/PTX cells. (b) Fluorescence intensity of Cy5.5-loaded PTX-ss-Zos @HCl NPs and Cy5.5-loaded PTX-ss-Zos@DSPE-PEG_{2k} NPs in 293T, L929 and MCF-7/PTX cells (1. Cy5.5-loaded PTX-ss-Zos@HCl NPs in HUVEC, 2. Cy5.5-loaded PTX-ss-Zos@HCl NPs in L929, 3. Cy5.5-loaded PTX-ss-Zos@DSPE-PEG_{2k} NPs in MCF-7/PTX, 4. Cy5.5-loaded PTX-ss-Zos@HCl NPs in MCF-7/PTX).

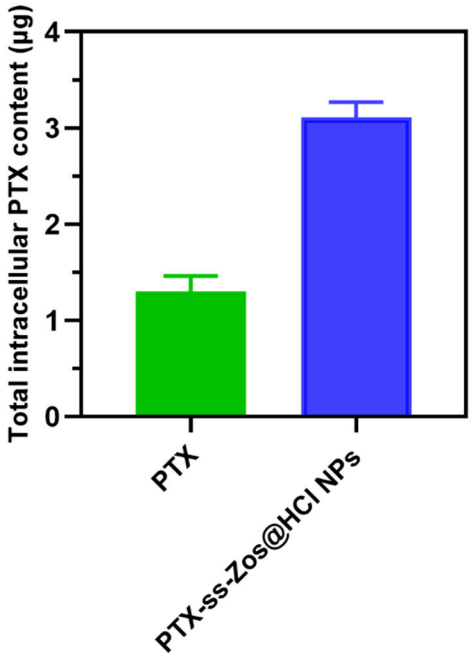

Figure S17. The intracellular content of PTX in MCF-7/PTX cells treated with free PTX and PTX-ss-Zos@HCl NPs respectively for 8 h

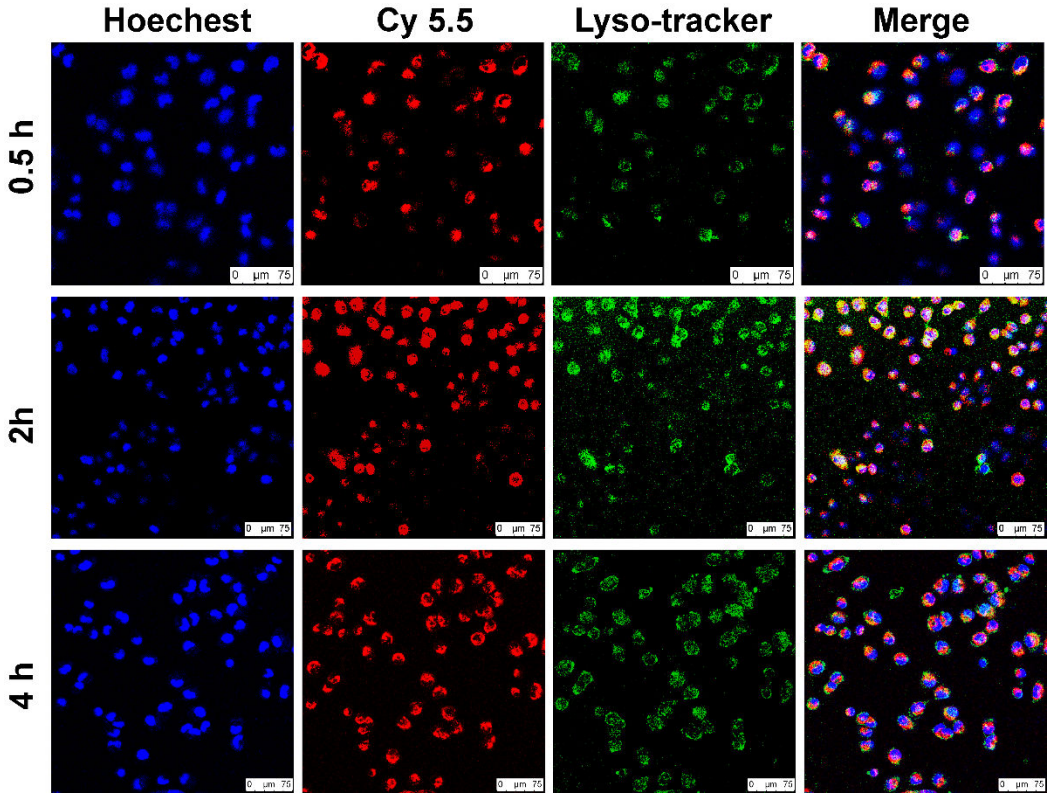

Figure S18. Confocal images of lysosomes and Cy 5.5 in MCF-7/PTX cells incubated with Cy5.5-loaded PTX-ss-Zos @HCl NPs for different times. Scale bars: 75 μm.

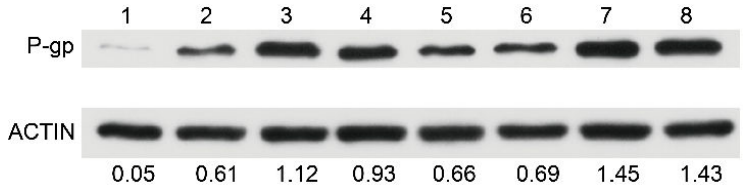

Figure S19. Western blot image of P-gp expression in untreated MCF-7 (1), MCF-7/PTX (2) cells and MCF-7/PTX cells treated with different drug formulations (3. PTX-ss-Zos conjugate, 4. Zos, 5. PTX-ss-Zos@HCl NPs, 6. PTX-ss-Zos@DSPE-PEG2k NPs, 7. PTX, 8. PTX/Zos mixture). The relative intensity ratios of P-gp/ACTIN are marked at the bottom.

The P-gp protein content in untreated MCF-7, MCF-7/PTX cells, and MCF-7/PTX cells after treatment with different drug formulations (PTX, Zos, PTX/Zos mixture, PTX-ss-Zos conjugate, PTX-ss-Zos@DSPE-PEG_{2k} NPs, PTX-ss-Zos@HCl NPs) was detected by western blot. The results showed that the P-gp expression was almost bare in sensitive MCF-7 cells, but significantly increased in drug-resistant MCF-7/PTX cells. The content of P-gp in drug-resistant cells was increased in various degrees after they were treated with different drug formulations, indicating that these drug formulations could stimulate the expression of P-gp in MCF-7/PTX cells. Among them, the expression level of P-gp in MCF-7/PTX cells treated with PTX and PTX/Zos mixture was nearly the same, and higher than those in MCF-7/PTX cells treated with Zos and PTX-ss-Zos conjugate. Meanwhile, the expression level of P-gp in MCF-7/PTX cells treated by nanodrugs (PTX-ss-Zos@DSPE-PEG_{2k} NPs and PTX-ss-Zos@HCl NPs) was only slightly higher than that of untreated MCF-7/PTX cells. This can be attributed to the fact that nanodrugs enter cells through endocytosis, bypass the efflux mechanism of P-gp, and then reduce the stimulation to P-gp.

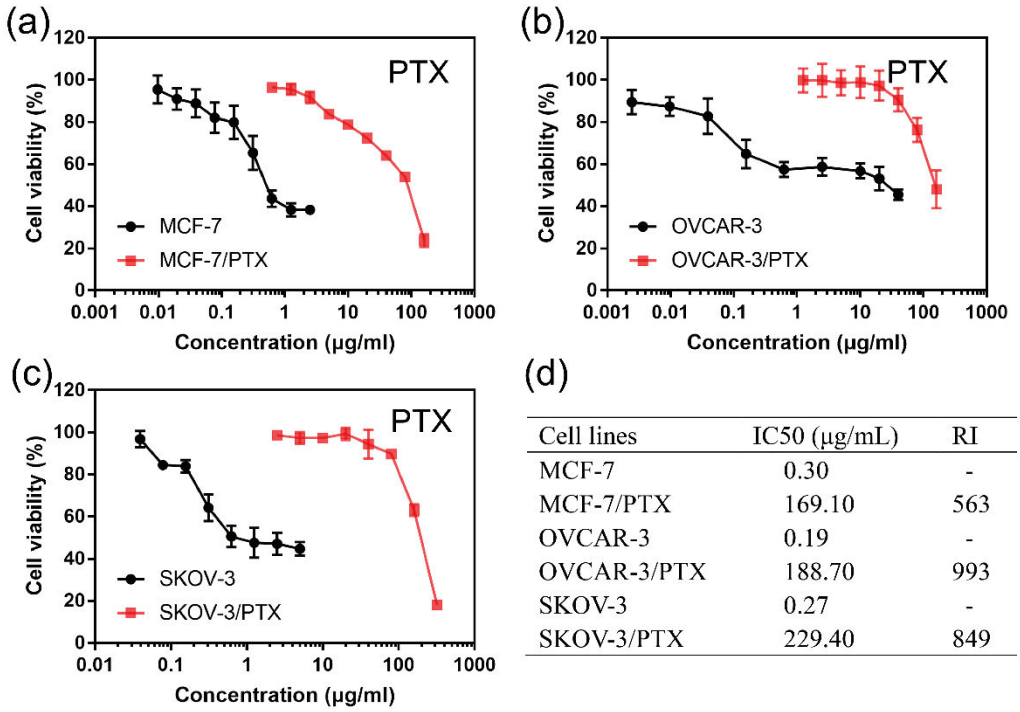

(d)

Cell lines	IC50 (μg/mL)	RI
MCF-7	0.30	-
MCF-7/PTX	169.10	563
OVCAR-3	0.19	-
OVCAR-3/PTX	188.70	993
SKOV-3	0.27	-
SKOV-3/PTX	229.40	849

Figure 20. *In vitro* cytotoxicity of PTX to (a) MCF-7 and MCF-7/PTX cells, (b) OVCAR-3 and OVCAR-3/PTX cells, and (c) SKOV-3 and SKOV-3/PTX cells by MTT assays. (d) The RI of PTX against MCF-7/PTX, OVCAR-3/PTX, and SKOV-3/PTX cells. RI = IC50 (PTX to drug-resistant cells)/IC50 (PTX to drug-sensitive cells).

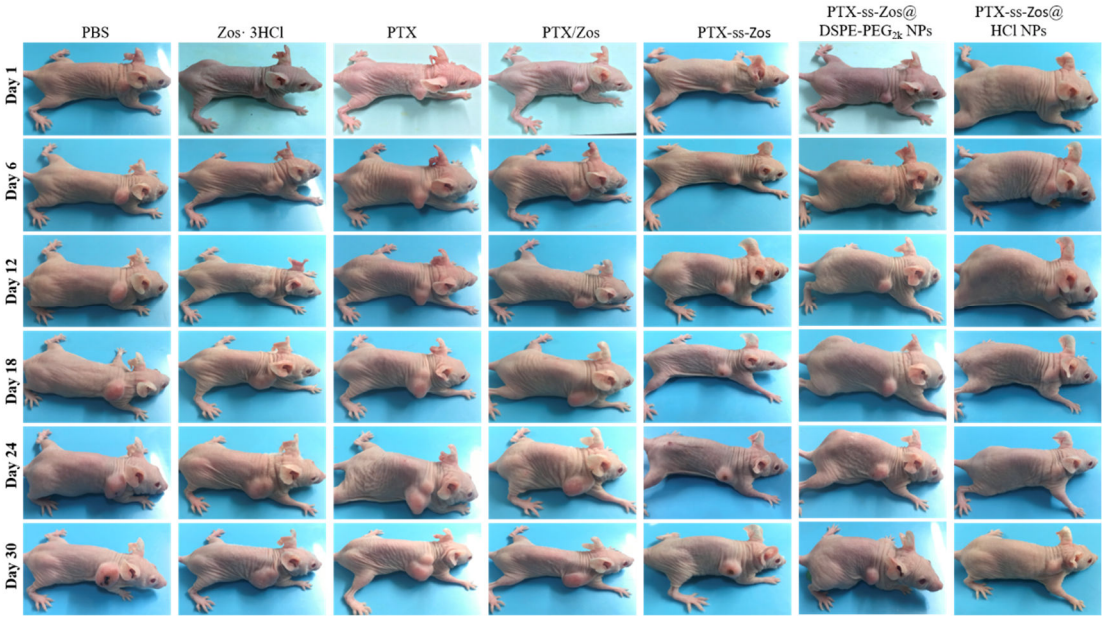

Figure S21. Images of the MCF-7/PTX-bearing nude mice during the predetermined treatments.

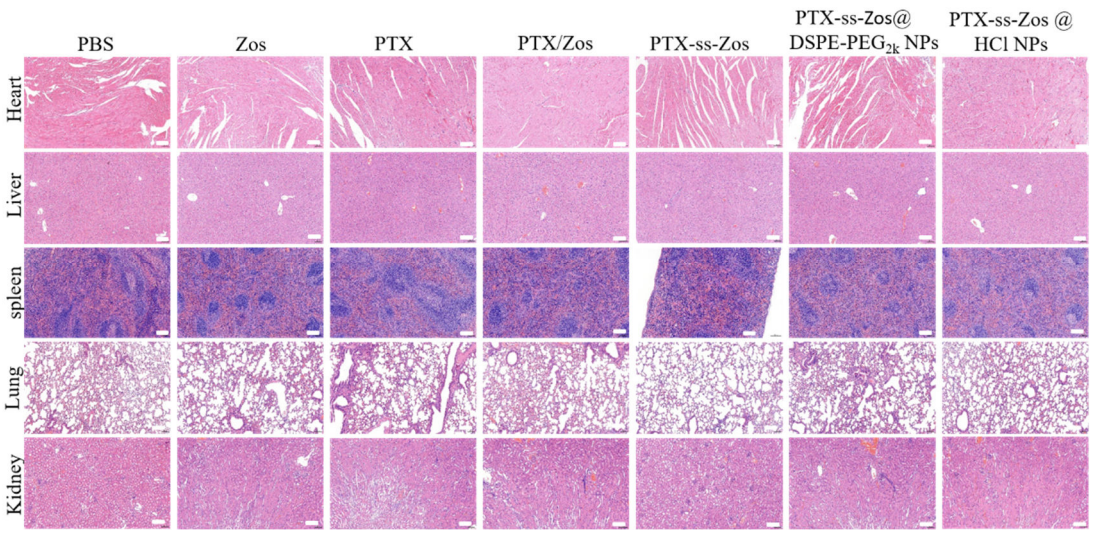

Figure S22. H&E staining of major organs (heart, liver, spleen, lung, kidney) of different drug formulations after 30 days of treatment. Scale bars: 100 μm.